THERMAL SHRINKAGE BASED VOLUME OF FLUID MODEL FOR PREDICTING THE VOIDS DURING SOLIDIFICATION OF LEAD

Niranjan Gudibande, Kannan Iyer*
Department of Mechanical engineering
Indian Institute of Technology Bombay,
Mumbai, 400076
India
niranjangn@iitb.ac.in; kiyer@iitb.ac.in

ABSTRACT

Radioactive materials are transported in hollow steel casks filled with Lead. Lead in these casks can melt in an accidental fire during transportation leading to an increase in its volume. This plastically deforms the steel shell housing the Lead. When the cask subsequently cools after the fire is extinguished, voids will be formed in the solidified Lead. The present work deals with the simulation of solidification with void formation in these transportation casks. In these simulations one has to deal with a solid-liquid and void-material interface. Solid-liquid movement during solidification is treated using a modified enthalpy method. The void which is formed in the solidified Lead is assumed to be a vacuum. Consistent with this assumption, the boundary conditions of zero pressure and zero-stress are imposed on the interface. The growth of void is handled using volume of fluid method. The methodology is first benchmarked by comparing the simulations with some experimental results available in literature. Simulations are then performed for solidification in the transportation cask to study the effect of orientation on the void formation. A methodology has been then developed to quantify the overall shielding effectiveness of the cask in terms of the total amount of radiation leaked.

KEYWORDS
Void formation, volume of fluid method, transport cask

1. INTRODUCTION

Solidification study is important in several areas such as casting, crystal growth, etc. The motivation for the present work arose from a need to analyze the effectiveness of steel casks, such as the one shown in Fig. 1(a) filled with Lead (which acts as shielding agent for the γ-rays emitted) in transporting radioactive materials. Such casks have to qualify in fire tests during which the cask is assumed to see a diesel fire for 30 minutes. While in fire, the Lead in the cask melts and the consequent volumetric expansion of Lead plastically deforms the cask. Once the fire is extinguished, the solidification process sets in and at the end of this process, shrinkage cavities are generated. A typical void formed in the cask is shown in Fig. 1(b). These cavities result in the degeneration of the shielding protection given by the Lead. Hence the prediction of the shape and location of shrinkage cavities is important. The present work is aimed in predicting these cavities.

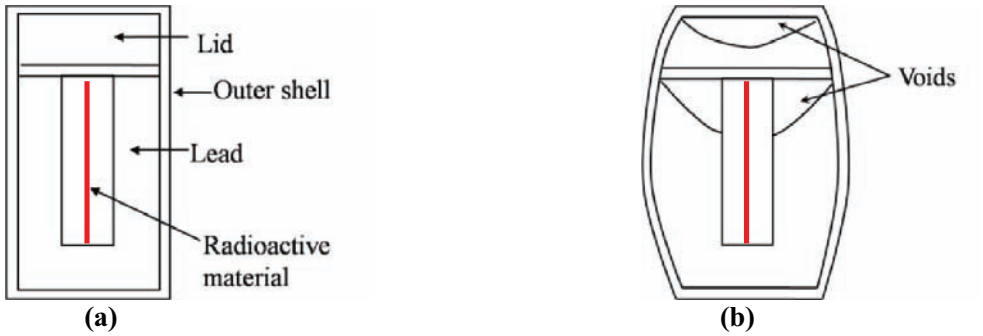

Figure 1 (a). A typical sketch of the cask used for gamma rays shielding (b). Voids formed in the plastically deformed cask.

Several models with varied level of complexity have been reported in the literature for the prediction of these voids. Thermal models (such as Sutaria et al [1]) solve for the temperature fields in the casting. Voids are assumed to be formed in the regions which solidify the last. Niyama et al [2] have proposed criteria function based on geometrical parameters to determine the regions which solidify the last, thus further simplifying the thermal models. These models can predict the probable locations of voids in the casting; however they cannot predict their final shape after solidification.

Trovant and Argyropoulos [3] and Pequet et al [4] have predicted the shrinkage cavity in castings using a volume shrinkage model. In this model, the liquid-void interface is assumed to be horizontal. The fraction of material which has solidified and hence the associated volume shrinkage is estimated at each time step by solving the energy equation. The level of the liquid in the control volumes which are at the top most portions (with respect to the gravity) of the casting are lowered to accommodate this volume shrinkage. Several investigators have analyzed the void formation using fixed as well as deforming grid methods. Kim and Ro [5], and Zhang et al. [6] have investigated pipe shrinkage using a deforming grid method. In this model the air-liquid interface was assumed to be flat. The velocity of the interface was obtained by applying a global mass balance for the entire system. This velocity is then used to move the interface. The air-liquid interface was assumed to be adiabatic. Bellet at al [7] have added an Arbitrary-Lagrangian-Eulerian module (ALE) to the commercial software THERCAST to simulate pipe formation in casting. Finite element method was used and the air-liquid interface was treated as adiabatic. Ehlen et al [8] have used an enthalpy method to simulate pipe formation in a binary alloy. The volume of fluid method of Hirt and Nichols [9] was used to model the free surface. Recently Sun and Garimella [10] have simulated the pipe formation in an explosive material both numerically and experimentally. Commercial software fluent was used to simulate the pipe growth. A volume of fluid method was used to handle the free surface.

From the survey, it was seen that either the problem of void formation is over simplified by heuristic approaches or when full simulation is carried out as done by Sun and Garimela [10], the mushy region is resorted to apply no slip boundary conditions in the solid-liquid interface. Such a treatment needs specification of arbitrary constants and the solutions are found to be sensitive to these constants [11]. In the present work a modified enthalpy method [12] is used to simulate solidification. The modified enthalpy method eliminates the mushy zone constants by first constructing a solid-liquid interface using the liquid fraction field. This interface is used to split the control volumes into solid and liquid control volumes. On the liquid split control volumes the no-slip boundary condition is directly imposed thus eliminating the use of mushy zone constants. The void is treated as a vacuum i.e. the pressure, stress at the interface is assumed to be zero. Justification for ignoring surface tension is provided in Section 4. The void growth is tracked using the volume of fluid method.

2. THE GOVERNING EQUATIONS

For simulating solidification with void growth, in addition to the solid-liquid interface, there exists a void-material interface. In control volumes which contain the void, interface boundary conditions will have to be imposed on them. These conditions can be derived by assuming the void to be vacuum. Consistent with the assumption that the void is vacuum, the stresses and the heat fluxes at the interface are assumed to be zero. The equations which govern the shrinkage defects are the continuity, momentum and the energy equations. These equations are derived in the following section. Consider a sample control volume shown in Fig. 2. In deriving these equations, the following nomenclature is followed. The surface area and the volume bound by the vertices ABCD in Fig. 2 are denoted as A and V respectively. The volume bound by the vertices JCDI is denoted as V^*, while the surface areas JC, CD and DI together is termed as A^*. The interface IJ is denoted as A_I.

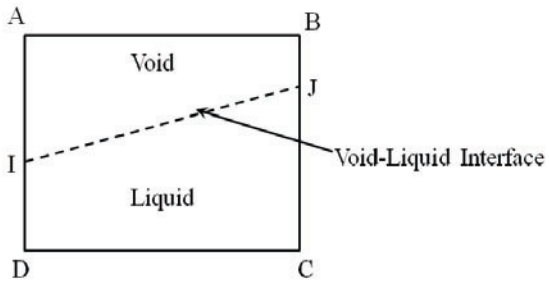

Figure 2. Control volume used in the derivation of the void growth equations

2.1 Mass Conservation equation

Consider a control volume shown in Fig. 2. The integral form of the mass conservation equation can be written as

$$\frac{d}{dt}\int_{V^*}\rho_L dV + \int_{A^*}\rho_L \mathbf{V}.\hat{n}dA = 0 \tag{1}$$

Here ρ_L is the density of the liquid and $\mathbf{V}$ is the velocity vector. Since the density of the void is assumed to be zero. The above equation can be written as

$$\frac{d}{dt}\int_{V}\rho_L(1-\alpha_P)dV + \int_{A}\rho_L(1-\alpha_A)\mathbf{V}.\hat{n}dA = 0 \tag{2}$$

Where α_P and α_A are the volume and the area averaged (on the control surface) void fractions respectively.

2.2 Conservation of momentum

Integral form of the conservation of momentum equation for the liquid part of the control volume in Fig. 2 is

$$\frac{d}{dt}\int_{V^*}\rho_L \mathbf{V}dV + \int_{A^*}\rho_L \mathbf{V}\mathbf{V}.\hat{n}dA = -\int_{A^*}P\hat{n}dA - \int_{A_I}P\hat{n}dA + \int_{A^*}\overline{\overline{\tau}}\hat{n}dA + \int_{A_I}\overline{\overline{\tau}}\hat{n}dA + \int_{V^*}\rho_L g dV \tag{3}$$

The interface is a region of zero pressure and zero stress, and thus the interface pressure and the stress terms in the above equation become zero. Incorporating the above simplifications, the momentum equation becomes

$$\frac{d}{dt}\int_{V^*}\rho_L \mathbf{V}dV + \int_{A^*}\rho_L \mathbf{V}\mathbf{V}.\hat{n}dA = -\int_{A^*}P\hat{n}dA + \int_{A^*}\bar{\bar{\tau}}\hat{n}dA + \int_{V^*}\rho_L g dV \tag{4}$$

By using the Stokes constitutive equations in simplifying the stress terms, the momentum equation can be written as

$$\frac{d}{dt}\int_{V}\rho(1-\alpha_P)\mathbf{V}dV + \int_{A}\rho(1-\alpha_A)\mathbf{V}\mathbf{V}.\hat{n}dA = -\int_{A}P(1-\alpha_A)\hat{n}dA + \int_{A}(1-\alpha_A)\mu\nabla\mathbf{V}\hat{n}dA + \int_{V}(1-\alpha_P)\rho_L g dV \tag{5}$$

2.3 Conservation of energy

Conservation of energy can be derived in a manner similar to the momentum equation. The heat flux across the void interface is assumed to be zero. The final enthalpy form of the energy equation is

$$\frac{d}{dt}\int_{V}\rho h(1-\alpha_P)dV + \int_{A}\rho h(1-\alpha_A)\mathbf{V}.\hat{n}dA = \int_{A}(1-\alpha_A)k\nabla T.\hat{n}dA \tag{6}$$

Here h and T are the enthalpy and the temperature of the material respectively.

2.4 Numerical Solution Methodology

In solving these governing equations, the finite volume methodology is employed. SIMPLE method of Patankar [13] is used with minor modifications. In control volumes not containing the void, the mass conservation (Eq. (2)) is used to derive the pressure correction equation, which helps in retrieving the pressure. In control volumes containing the void, the pressure correction is set to zero and mass conservation equation (Eq. (2)) is used to obtain the void fraction. In control volumes containing the interface, if the convective terms of the void growth in Eq. (2) are discretized using convectional convection schemes, such as upwind, central, second order upwind etc., the void fraction α_P becomes diffuse. To avoid this, the mass conservation equation has to be solved by using geometric advection algorithm [14-15], which is commonly used in two phase flow simulations.

3. RESULTS AND DISCUSSIONS

Before attempting the solution to the solidification of the casks, a few benchmark problems were attempted. The first problem involves solidification of Tin without accounting for the volume contraction. This is followed by simulation of solidification of Octadecane and TNT with void formation. These are described in the following section.

3.1 Solidification of Tin

To benchmark the methodology used for solving solidification, a benchmark problem of solidification of Tin without accounting for volume contraction is attempted. Experimental results of Wolff and Viskanta [16] are available for such a situation. Although there are volume contractions in the actual experiment, this has negligible influence on the location of the solid-liquid front. Molten Tin initially at a temperature higher than its melting temperature is placed in a rectangular container. The right wall is subjected to a temperature lower than the melting temperature while the left wall is placed at the initial temperature itself. A solid-liquid interface forms at the right wall and moves to the left as the time progresses. A

Cartesian mesh consisting of 80x80 control volumes was found adequate to get grid insensitive results. Solid-liquid interface at various times are compared with the experimental results of Wolff and Viskanta [16] and numerical results of Li et al [17] in Fig.3. It is seen that there is comparable agreement between the present numerical results and the numerical results of Li et al [17]. The discrepancy between the numerical results the experimental results of Wolff and Viskanta [16] can be attributed to the technique employed to determine the solid-liquid interface. The solid-liquid interface was determined by Wolff and Viskanta [16] using a probe to poke the Tin to physically feel the solid-liquid interface. Since Tin at its melting temperature is soft and the molten liquid tin is viscous, there is uncertainty in the measurement of the solid-liquid interface.

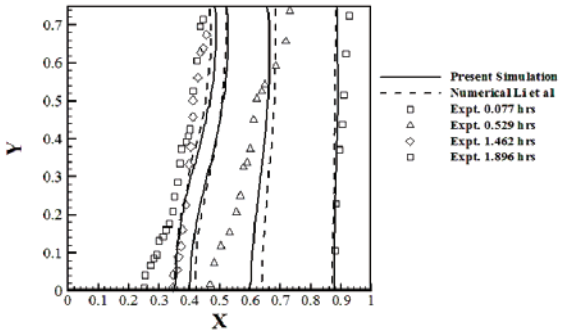

Figure 3. Comparison of Solid-liquid fronts at various times between the present simulation with numerical results of Li et al [17] and experimental results of Wolff and Viskanta [16].

3.3 Solidification of Octadecane

Simulation of solidification of n-Octadecane with the formation of voids is then carried out. Ho and Viskanta [18] have performed these experiments in a rectangular cavity. Octadecane initially at a temperature slightly higher than its melting temperature is placed in a square cavity with an open top. Solidification was initiated by lowering the temperature of the side and the bottom wall to a temperature lower than the melting temperature. Solid-liquid and void-material interface were recorded. Fig. 4 shows the comparison of the solid-liquid and the void-material interface at various times between the experimental results of Ho and Viskanta [18] and the present numerical results. There is fair agreement between the two results.

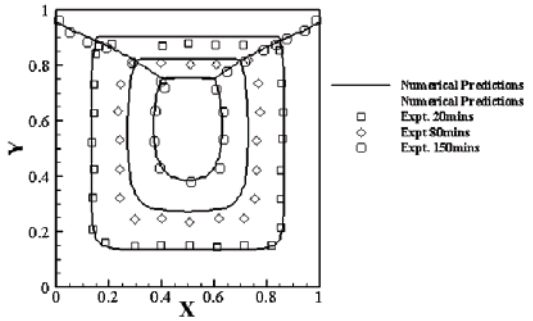

Figure 4. Comparisons of Solid-liquid and void-material interfaces during the solidification of n-Octadecane between the present results and the experimental results of Ho and Viskanta [18].

3.4 Solidification of TNT

Simulation is also performed for predicting the pipe shrinkage during solidification of TNT (trinitrotoulene). Sun and Garimella [10] have performed both numerical simulations and experiments to study the void growth during solidification of TNT. TNT has a sharp melting point of 354 K and thus behaves as a pure material. In the experiments performed by Sun and Garimella [10], TNT was placed in a cylindrical mould whose aspect ratio (diameter to eight) was 1/5.65. TNT was initially at a temperature slightly higher than the melting point. The TNT was allowed to solidify by controlling the temperature of the steam heaters placed along the sides and the bottom of the cylindrical mould. The measured temperature on the top, bottom and side surfaces were taken as the boundary conditions for the simulation. Simulations were performed in the present study, by considering air as a void, which implies that air-TNT interface is assumed to be insulated. While Fig. 5(a) shows the present numerical results compared with the numerical results of Sun and Garimella [10], Fig. 5(b) shows their experimental and numerical results. It can be seen that while the present numerical results compare favorably with the numerical results of Sun and Garimella [10], there is some discrepancy between the experimental results and the numerical results. Particularly the smaller voids have not been captured. Sun and Garimella [10] explain this discrepancy as being due to the presence of dissolved gases in the material and the presence of thermocouple rakes inside the mould which could cause multiple nucleations of voids during solidification.

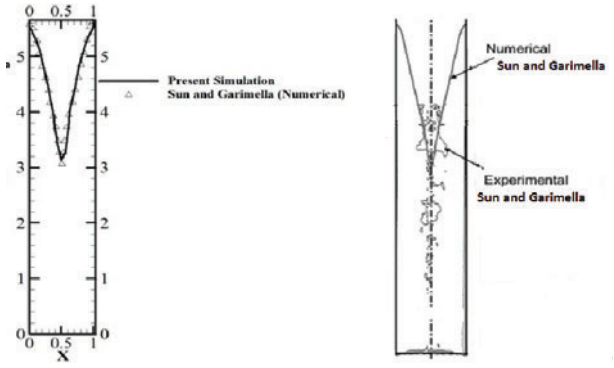

(a) **(b)**

Figure 5. Comparisons between (a) the present numerical results and the numerical results of Sun and Garimella [10]; (b) their numerical and the experimental results.

3.5 Effect of radiation on the void formation

The benchmark simulations for void formation presented in the previous section involved solidification of low melting point substances. In these situations, the radiation heat loss from the void-material interface is negligible. Lead has a relatively higher melting temperature of 327^{O}C and hence one has to determine if radiation heat transfer is significant. In real casks due to the presence of a thick outer steel shell, the void interacts radiatively to the shell. Due to the conjugate heat transfer in the steel shell, the shell is relatively hot. Thus the radiation effect may be negligible. To understand the effect of radiation, a simulation was performed on the solidification of Lead in a circular cylinder of 0.5m inner height and 0.25m inner diameter and a uniform thickness of 0.01m. Lead was initially at a superheat of 100^{O}C and the outer walls radiated to the atmosphere at 30^{O}C. This results in a void such as that shown in Fig. 6(a). Radiation transfer from the void surface of area dA (refer Fig. 6(a)) to the steel top plate of area A_p will be

$$Q_f = \frac{\sigma\left(T_V^4 - T_P^4\right)dA}{\frac{1-\varepsilon_P}{\varepsilon_P A_P}dA + \frac{1}{F_{VP}} + \frac{1-\varepsilon_V}{\varepsilon_V}} \tag{7}$$

Here σ ε_V and ε_P are the Stefan Boltzmann's constant, emissivity of the void and emissitivity of plate respectively. T_V is the local temperature of the void-liquid interface and T_P is the average temperature of the plate respectively. In Eq.7 dA/A_P is small and thus the first term in the denominator of Eq.7 is neglected. Eq. 7 involves calculation of F_{VP} which is view-factor from the void to the top plate. Calculation of F_{VP} is complex. In the present simulation F_{VP} is set to be unity. By doing so the radiation heat transfer from the void to the top plate is over estimated. Fig.6 (b) and (c) show the void formed in Lead with and without accounting for the radiation heat transfer, it is found to be nearly identical. Since this simulation was performed by over estimating the radiation transfer from void to plate and yet the voids seem to be insensitive to radiation. Thus it may be concluded that radiation heat transfer between the cask and the void can be neglected. Further analysis has been carried out with this assumption.

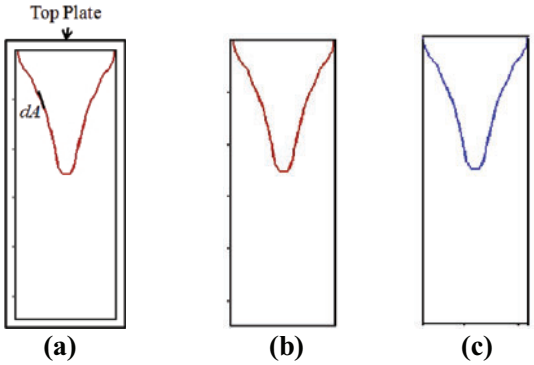

Figure 6. (a) Schematic of the radiation interaction between the Void-Lead interface and top surface of the cask; (b) Void-Lead interface with radiation; (c) Void-Lead interface without radiation

4. SIMULATIONS OF SOLDIFICATION IN TRANSPORTATION CASKS

Having benchmarked the methodology for simulating solidification with void formation, simulations were then performed on actual transportation cask. The sketch of the cask with the dimensions employed in the present study is shown in Fig. 7(a). As described in the Section 1 of this paper, the cask when subjected to fire will undergo a plastic deformation. To accurately quantify the effectiveness of the cask for gamma ray shielding it is realistic to predict the voids distribution in the deformed cask. To predict the shape of the cask after it has undergone plastic deformation, a commercial code, Ansys, has been employed. When the solid Lead melts it undergoes 5.99% increase in its volume. To determine the shape of the cask after it has undergone plastic deformation the pressure inside the cask was iteratively adjusted such that it expanded to 5.99% of its initial volume. The pressure inside the cask was then lowered to zero to relax the cask. This final shape of the cask is employed for subsequent solidification analysis. The rationale behind relaxing the cask is explained as follows. As the Lead solidifies the pressure in the liquid becomes zero before the initiation of the void. This lowering of pressure will relax the deformed cask due to the elastic component of the deformation. The final shape of the cask is shown in Fig. 7(b).

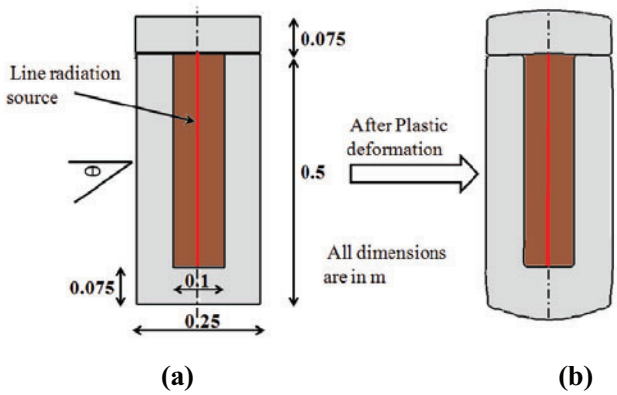

Figure 7. Sketch of the cask (a) before deformation (b) after deformation due to melting and subsequent relaxation.

In a diesel fire scenario after the diesel driven transportation vehicle meets with an accident, the cask may take an arbitrary orientation with respect to gravity The aim of this paper is to study the effect of orientation (refer Fig. 7(a) for the definition of the angle of orientation) on the void formation. The Lead in the cask was assumed to be initially at a superheat of 100^{O} C. The outer surface of the cask was assumed to radiate to atmosphere at a temperature of 30^{O} C. When the cask starts to solidify, a void is initiated in the cask where there is minimum pressure. Since the pressure variation due to natural convection current in the liquid metal is small, the pressure distribution is nearly hydrostatic. Thus the voids are initiated in the top portions (relative to gravity) of the cask. Simulations were performed in mesh consisting of 100×100×200 grid points (200 points along the axis of the cask). Each simulation took about 150 hrs of computation time on an Intel Xeon E31230 machine. The final shape of the void for different angles of orientation is shown in Fig. 9. The voids formed in the cask have a complex three dimensional structure. The voids shown in Fig. 9 correspond to the plane which has the maximum depth of the void. This plane has its normal perpendicular to the gravity. Fig. 8 shows a 3d isometric view of the cask and the plane where the voids are depicted. It can be seen in Fig. 9 that the voids are formed in the top portions of cask as expected.

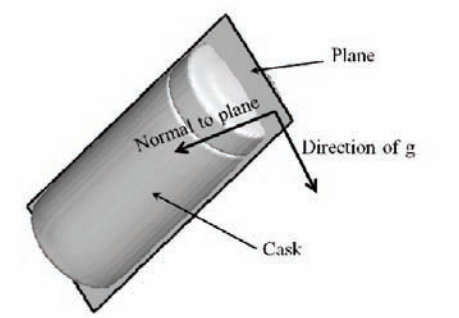

Figure 8. Figure showing the plane along which the void-solid interface is shown

In these simulations the surface tension forces were neglected. Since the voids formed during solidification are large a void free-surface is formed under the action of the gravitation force. To quantify this we compute the Bond number which is the ratio of body force to the surface tension force

$$Bo = \frac{\rho g L^2}{\sigma} \tag{8}$$

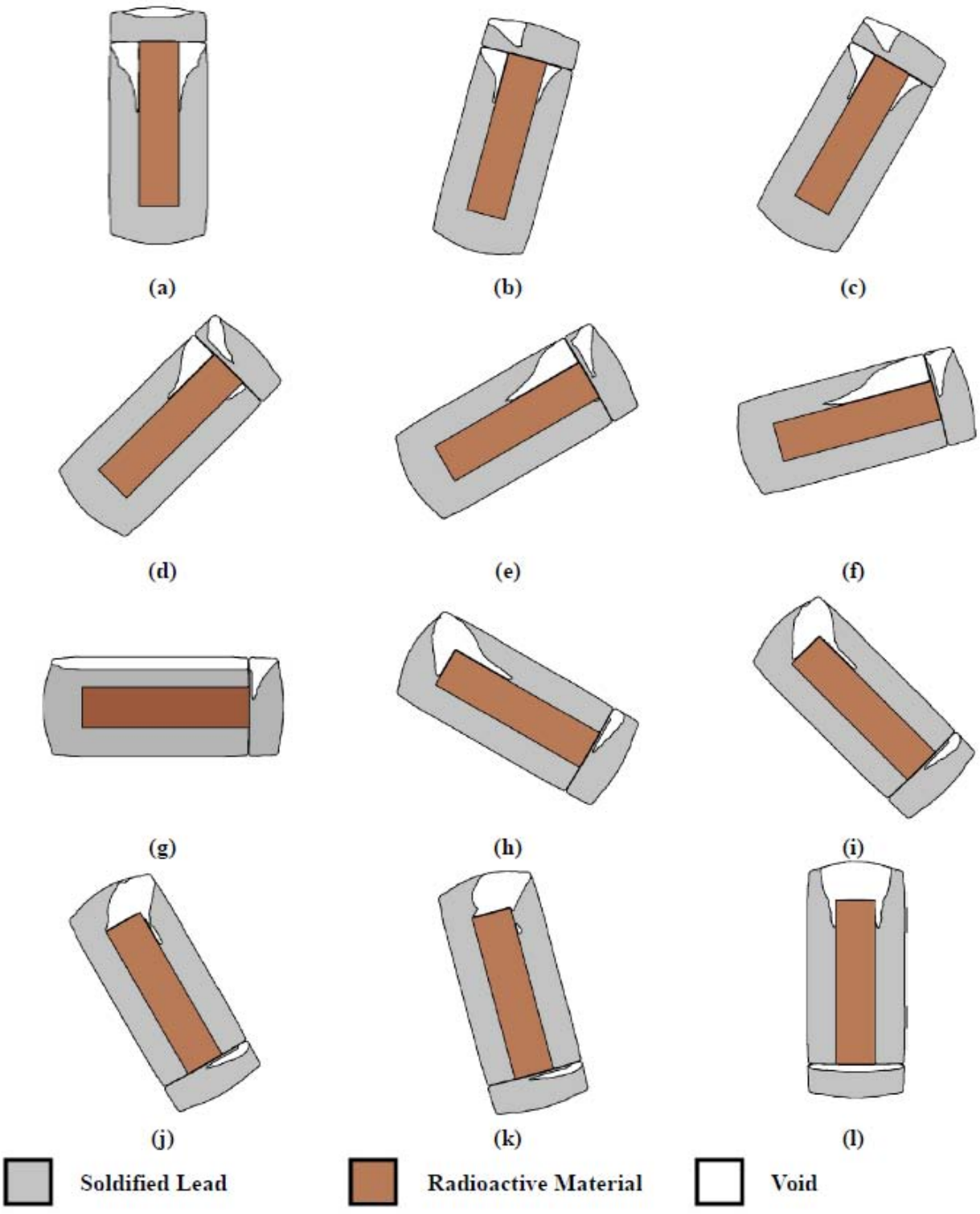

Figure 9. The void material interface after complete solidification for various angle of orientation (a) 90º (b)75º (c)60º (d)45º (e)30º (f)15º (g)0º (h) -30º (i) -45º (j) -60º (k) -75º (l) -90º.

In Eq.8, σ is the surface tension coefficient and L is a characteristic length scale. By choosing the length scale as the cube-root of the void volume the Bond number in the body of the cask and the lid were found to be 2775 and 866 respectively. These large numbers suggests that surface tension forces are negligible in the present study. To quantify the shielding effectiveness of the cask, the flux of the photons leaving the surface of the cask has to be determined. For better visual representation, a cylinder is circumscribed over the deformed cask as shown in Fig. 10. The gamma ray photon flux on the lateral surface of this cylinder as well as the top and bottom surfaces can then be represented as contour plots. To carry out this analysis radioactive source is assumed to be a line source as shown in Fig.10.

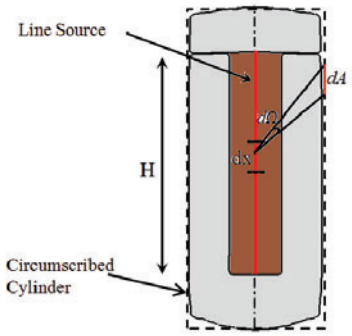

Figure 10 Cask with a linear source showing the linear element and the circumscribed cylinder

In the presence of solid Lead the radiation emitted by this linear source gets attenuated as it reaches the surface of the cylinder. The photon flux, ϕ, at the area dA on the circumscribed cylinder due to a small element dx at a distance x from the base of the linear source is given by [19]

$$d\phi = \frac{S'dx}{4\pi r^2} B(\mu L) exp(-\mu L) \tag{9}$$

Here L is the thickness of lead intercepted by the photons, r is the distance between the small linear element and the area dA, μ is the linear absorption coefficient of Lead and B is the buildup factor which accounts for the scattering effects. The buildup factor is usually represented in the Taylor form [19] i.e.

$$B(\mu L) = A\,exp(-\alpha_1 \mu L) + (1-A)exp(-\alpha_2 \mu L) \tag{10}$$

The values of μ, α_1, α_2 and A depend on the energy of the gamma ray source. Shultis [20] reports that nearly 65% of radioactive sources in a typical cask emit gamma ray in the range of 0.6-0.8 MeV. Corresponding to an energy of 0.7 MeV the values of μ, α_1, α_2 and A have been obtained as 1.29 /cm, -0.030, 0.31 and 1.68 respectively from [19]. The total flux of photons incident on the area dA can be obtained by integrating the above equation over the entire length of the linear radioactive source

$$\phi = \int_0^H \frac{S'dx}{4\pi r^2} \left[A\,exp(-(1+\alpha_1)\mu L) + (1-A)exp(-(1+\alpha_2)\mu L)\right] \tag{11}$$

It may be noted that L and r depends on the direction of the path of the photons. Further, in the absence of Lead the flux of the photons is

$$\phi_O = \int_0^H \frac{S' dx}{4\pi r^2} \tag{12}$$

ϕ_O can be used to non-dimensionless ϕ in Eqn. 11 as

$$\eta = \frac{\phi}{\phi_O} \tag{13}$$

Higher values of η (Intensity ratio) would indicate decrease in effectiveness of shielding. The η field on the surface of the circumscribed cylinder without pore is shown in Fig.11 while the η field for all the angle of orientation (with void) is shown in Fig.12. The circular contours shown on the top and the bottom of the cask are the photon fluxes on the top and the bottom circular plate of the circumscribed cylinder. The lateral surface of the cylinder has been opened up and the flux contour on this surface is shown to the side of the cask. To better appreciate the values of η observed in the Fig.12, the effectiveness of the cask in the absence voids shown in Fig.11 can be compared. Peak η has significantly increased (almost by two orders of magnitude) due to the voids. It can be seen in the contour plots of Fig. 12 that the γ-ray flux is maximum in the portions of the cask which has maximum depth of void as expected. The peak intensity ratio in most the angles of orientation is reasonably high which suggests that the effectiveness of cask to shield radiation has been compromised. An interesting feature observed in contour plots of Fig.12 is that relatively less γ-rays stream out of the lid portion of the cask. The lid and the body of the cask are considered as two separate fluid-tight compartments (as the shell of the cask body and the lid are made of stainless steel and the stress developed in the compartments is below the breaking stress, thereby eliminating the formation of cracks). Thus after solidification, voids are formed separately instead of a single large void. This distribution of voids tends to decrease the radiation leakage. This observation suggests that a cask which can be made by assembling several fluid-tight compartments may lead to distributed void formation and thus fare better in shielding against radiation in an accidental fire.

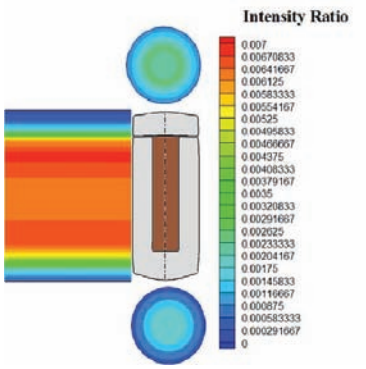

Figure 11 The contours of Intensity ratios without pore

5. CONCLUSIONS

In the present work a modified enthalpy method along with volume of fluid method is used to simulate the solidification with void growth. Some benchmark results were presented to validate the methodology. Simulations were then performed on solidification of plastically deformed casks and the effect of the orientation on the void formation was studied. The effectiveness of the cask in shielding the radiation was further quantified using a ray tracing method. It was observed that the effectiveness of cask to shield radioactivity was compromised in several angle of orientation.

ACKNOWLEDGMENTS

The work reported in this paper was partially funded by BARC (Bhabha Atomic Research Center) under a research grant.

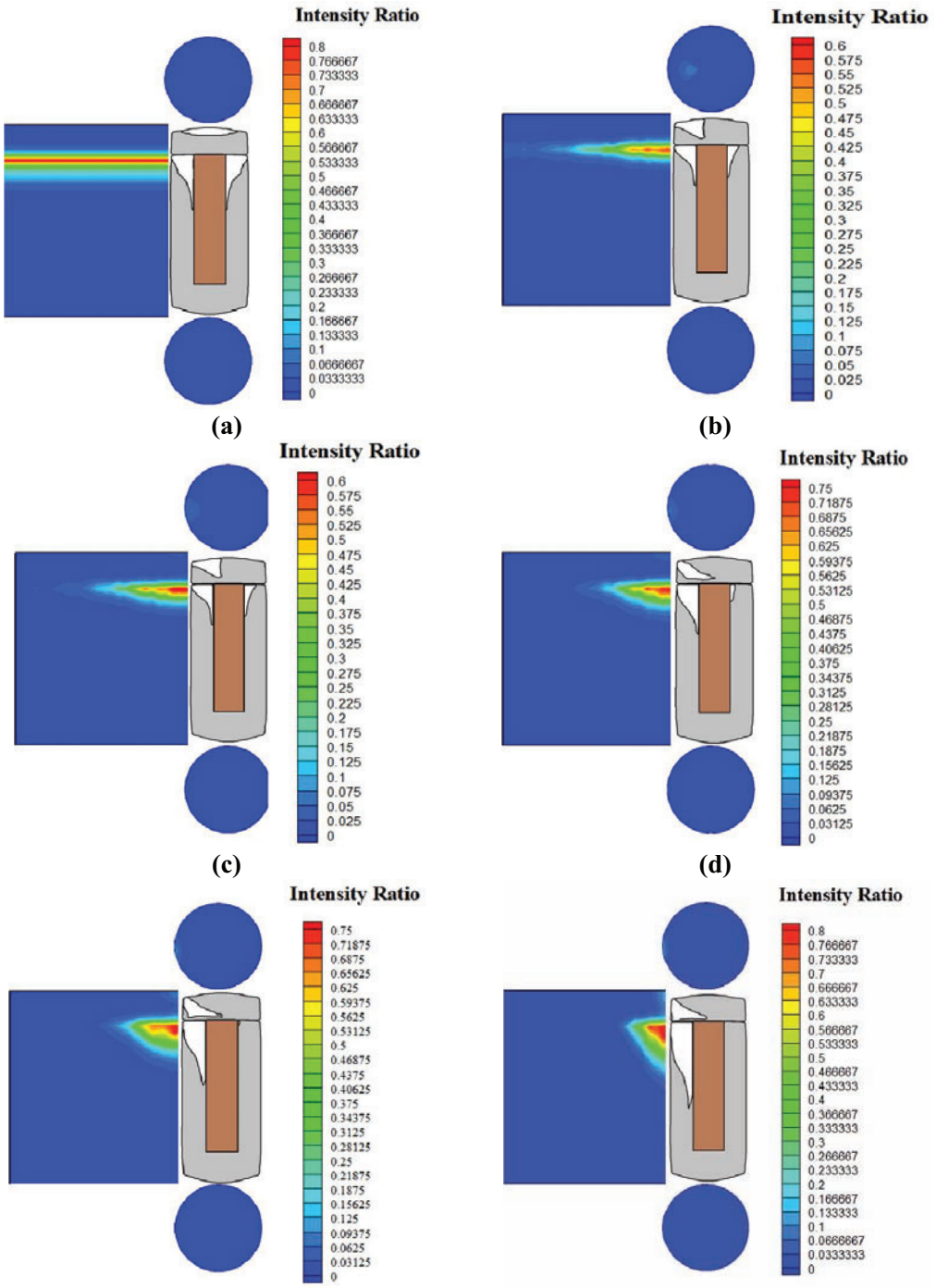

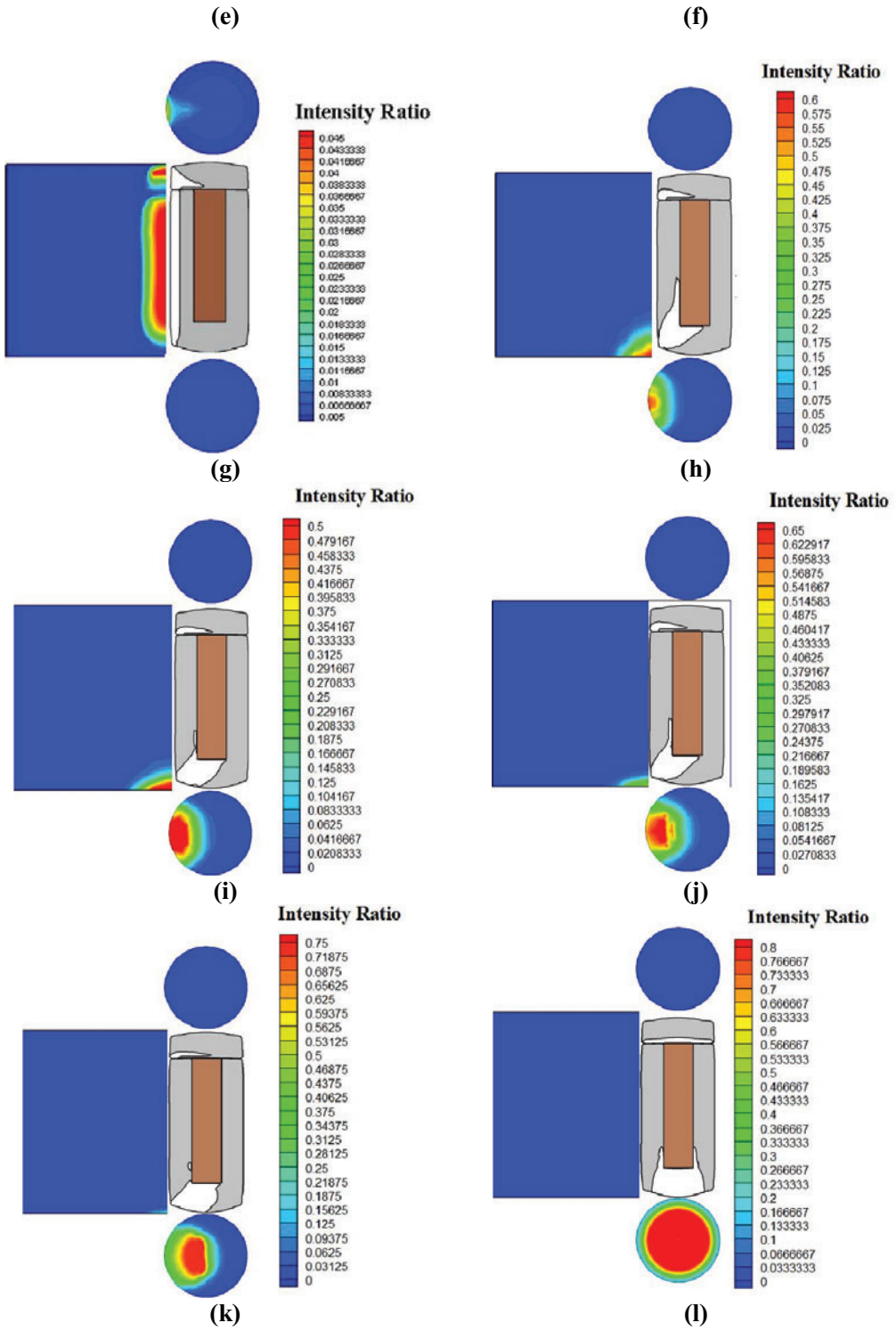

Figure 12 The contours of Intensity ratios for various angle of orientation (a) 90^{O} (b)75^{O} (c)60^{O} (d)45^{O} (e)30^{O} (f)15^{O} (g)0^{O} (h) -30^{O} (i) -45^{O} (j) -60^{O} (k) -75^{O} (l) -90^{O}.

REFERENCES

1. M. Sutaria, ,V. H. Gada, A. Sharma and B. Ravi , "Computation of feed-paths for casting solidification using level-set-method," *Journal of Materials Processing Technology*, **212**(6), pp. 1236-1249 (2012).
2. E. Niyama, T. Uchida, M.Morikawa and S. Saito, "A method of shrinkage prediction and its application to steel casting practice,"*International Journal of casting*, **9**, pp. 52-63 (1982).
3. M. Trovant and S.A. Argyropoulos, "Mathematical modelling and experimental measurements of shrinkage in the casting of metals,"*Canadian Metallurgical Quarterly*, **35**(1), pp.75-84 (1992).
4. C. Pequet, M. Gremaud andM.Rappaz,"Modelling of microporosity, macroporosity, and pipe-shrinkage formation during the solidification of alloys using a mushy-zone refinement method: Applications to aluminium alloys,"*Metallurgical and Materials Transactions A: Physical Metallurgy and Materials Science*, **33**(7)pp.2095-2106 (2002).
5. C.J. Kim and S.T. Ro, "Shrinkage Formation during the Solidification Process in an Open Rectangular Cavity," *Journal of Heat Transfer, Trans. ASME,***115**(4)**,** pp.1078-1080 (1993).
6. H. Zhang, V. Prasad and M. K. Moallemi, "Numerical algorithm using multizone adaptive grid generation for multiphase transport processes with moving and free boundaries,"*Numerical Heat Transfer, Part B: Fundamentals*, **29**(4), pp. 399-421 (1996).
7. M. Bellet, O. Jaouen, and I. Poitrault, "An ALE-FEM approach to the thermomechanics of solidification processes with application to the prediction of pipe shrinkage,"*International Journal of Numerical Methods for Heat and Fluid Flow*, **15**(2), pp. 120-142 (2005).
8. G. Ehlen, A. Ludwig, P.R. Sahm and P. R.Bührig-Polaczek,"Split-solid-model to simulate the formation of shrinkage cavities and macrosegregations in steel casting," *Modeling of Casting, Welding and Advanced Solidification Processes*, pp.285-292 (2003).
9. C.W. Hirt, and B.D. Nichols, "Volume of fluid (VOF) method for the dynamics of free boundaries,"*Journal of Computational Physics*, **39**(1), pp. 201-225 (1981).
10. D. Sun and S.V. Garimella, "Numerical and experimental investigation of solidification shrinkage," *Numerical Heat Transfer; Part A: Applications*, **52**(2), pp. 145-162 (2007).
11. H. Shmueli, G. Ziskind, and R. Letan, R., "Melting in a vertical cylindrical tube: numerical investigation and comparison with experiments," *International Journal of Heat and Mass Transfer*, **53**(19), pp. 4082-4091 (2010).
12. N.N Gudibande, N. N, K.N. Iyer, "Modified enthalpy method for the simulation of melting and solidification," *Sadhana- Academy Proceedings in Engineering Sciences,***36**(6) pp. 1259-1285 (2013).
13. S.V Patankar,pp. 126, *Numerical Heat Transfer and Fluid Flow,* Hemisphere, Washington, D.C., USA (1980).
14. W.J. Rider, W. J., and D.B. Kothe, D. B., "Reconstructing volume tracking,"*Journal of Computational Physics*, **141**(2), pp. 112-152 (1998).
15. J.E. Pilliod and E.G. Puckett, "Second-order accurate volume-of-fluid algorithms for tracking material interfaces,"*Journal of Computational Physics*, **199**(2), pp. 465-502 (2004).
16. F. Wolff and R. Viskanta, "Solidification of a pure metal at a vertical wall in the presence of liquid superheat,"*International Journal of Heat and Mass Transfer,***31**(8), pp. 1735-1744 (1998).
17. C. Li, S.V. Garimella and J.E. Simpson, "Fixed-grid front-tracking algorithm for solidification problems, part II: Directional solidification with melt convection,"*Numerical Heat Transfer, Part B: Fundamentals*, **43**(3) pp. 143-166 (2003).
18. C.J. Ho and R. Viskanta, "Experimental Study of Solidification heat transfer in an open rectangular cavity,"*Journal of Heat Transfer,***105**(3), pp. 671-673 (1983).
19. J.R Lamarsh and A.J. Baratta, pp 58, *Introduction to nuclear engineering*, Prentice-Hall Inc., Upper Saddle River, New Jersey, USA. (1975).
20. J.K. Shultis, *Radiation Analysis of a Spent Fuel Storage Cask*, Report 290 Engineering Experimental Station Kansan State University Kansas (2000).